
Multi-Output Convolution Spectral Mixture for Gaussian Processes

Kai Chen

Shenzhen Institutes of Advanced Technology, Chinese Academy of Sciences
Shenzhen College of Advanced Technology, University of Chinese Academy of Sciences
Institute for Computing and Information Sciences, Radboud University
kchen@cs.ru.nl

Perry Groot

Institute for Computing and Information Sciences, Radboud University
perry.groot@science.ru.nl

Jinsong Chen

Shenzhen Institutes of Advanced Technology, Chinese Academy of Sciences
js.chen@siat.ac.cn

Elena Marchiori

Institute for Computing and Information Sciences, Radboud University
elenam@cs.ru.nl

Abstract

Multi-output Gaussian processes (MOGPs) are recently extended by using spectral mixture kernel, which enables expressively pattern extrapolation with a strong interpretation. In particular, Multi-Output Spectral Mixture kernel (MOSM) is a recent, powerful state of the art method. However, MOSM cannot reduce to the ordinary spectral mixture kernel (SM) when using a single channel. Moreover, when the spectral density of different channels is either very close or very far from each other in the frequency domain, MOSM generates unreasonable scale effects on cross weights which produces an incorrect description of the channel correlation structure. In this paper, we tackle these drawbacks and introduce a principled multi-output convolution spectral mixture kernel (MOCSM) framework. In our framework, we model channel dependencies through convolution of time and phase delayed spectral mixtures between different channels. Results of extensive experiments on synthetic and real datasets demonstrate the advantages of MOCSM and its state of the art performance.

1 Introduction

Gaussian processes (GPs) [1, 2] are an elegant Bayesian approach to model an unknown function. They provide regression models where a posterior distribution over the unknown function is maintained as evidence is accumulated. This allows GPs to learn complex functions if a large amount of evidence is available and makes them robust against overfitting in the presence of little evidence. A GP can model a large class of phenomena through the choice of its kernel which characterizes one's assumption on how the unknown function autocovaries [1]. The choice of the kernel is a core aspect of GP design, since the posterior distribution can significantly vary for different kernels.

As a consequence, various kernels, e.g., Squared Exponential, Periodic, Matérn, and kernel design methods have been proposed [2].

The extension of GPs to predict multiple output variables (or channels, tasks) simultaneously is known as multi-output Gaussian processes (MOGPs). Usually MOGPs are also called multi-task Gaussian processes (MTGPs). For convenience, in some cases, MOGPs and MTGPs are used alternately. MOGPs model temporal or spatial relationships among infinitely many random variables, as scalar GPs, but also account for the statistical dependence across different sources of data (or channels) [3]. How to choose an appropriate kernel to jointly model the cross covariance between channels and auto-covariance within each channel is the core aspect of MOGPs design.

Early approaches to MOGPs, like Linear Model of Coregionalization (LMC [4] [5] [6], focused on linear combinations of shared kernels. More expressive methods like the multi-kernel method [7] and the convolved latent function framework [8] consider convolution to construct cross covariance functions, and assume that each channel has its own kernel. Recently spectral mixture (SM) kernels have been used and extended for MOGPs resulting in a principled method for constructing cross-covariance functions which are easier to interpret. Initially, the SM-LMC kernel [9, 10] was proposed, which uses shared spectral mixtures. A more flexible kernel is the Cross-Spectral Mixture (CSM) kernel [11], which considers the power and phase correlations between multiple outputs. The CSM kernel, however, cannot capture time delayed cross correlations between channels. The Multi-Output Spectral Mixture kernel (MOSM) [3] addresses this limitation, but has some other drawbacks. First, MOSM cannot reduce to the ordinary spectral mixture kernel (SM) when using a single channel. Second, when the spectral density of different channels is either very close or very far from each other in the frequency domain, MOSM generates unreasonable scale effects on cross weights which produces an incorrect description of the channel correlation structure.

In this paper, in order to address these drawbacks in MOSM, we propose a multi-output convolution spectral mixture kernel (MOCSM) framework based on convolution of spectral mixtures which is a direct generalization of single task GP that better captures cross covariance than MOSM. MOCSM shows a stronger ability of discovering channel correlation in each component. Particularly the cross weights reflecting channel correlations in MOCSM are more accurate than MOSM. Although MOCSM and MOSM have the same parameter space, MOCSM gives a more accurate closed form of multi-output spectral mixture kernel. The aforementioned approaches can be seen as specific instances of MOCSM.

The paper is mainly structured as follows. In Section 3 we show how to construct cross spectral mixtures with time and phase delay through convolution, extend the cross spectral mixtures to multi-output scenario, and compare MOCSM and MOSM. In Section 4 we describe further the difference between MOCSM and aforementioned cross SM approaches for MOGPs. Section 5 discusses the experiments of our approach on synthetic and real dataset. Some summary, concluding remarks and future work on this topic are given in the final Section 6.

2 Background

We start with some background information on GPs, multi-output GPs, and spectral mixture kernels.

2.1 Gaussian processes

A Gaussian process defines a distribution over functions, specified by its mean and covariance function [2]. The mean function $m(x)$ and covariance function $k(x, x^\top)$ can be written as

$$m(x) = \mathbb{E}[f(x)] \tag{1}$$

$$k(x, x^\top) = \mathbb{E}[(f(x) - m(x))(f(x^\top) - m(x^\top))]. \tag{2}$$

where x is an arbitrary input variable in \mathbb{R}^P . The covariance function k mapping two random variables into \mathbb{R}^P , is applied to construct a positive definite covariance matrix, here denoted by K . Given $m(x)$ and $k(x)$, we can define a GP as

$$f(x) \sim \mathcal{GP}(m(x), k(x, x^\top)). \tag{3}$$

Without loss of generality we assume the mean of a GP to be zero. By placing a GP prior over functions through the choice of kernels and parameter initialization, and the training data, we can

predict the unknown value y_* and its variance $\text{var}(y_*)$ (that is, its uncertainty) for a test point x_* using the following key predictive equations for GP regression [2]:

$$m(y_*) = K^\top(\mathbf{x}, x_*)(K(\mathbf{x}, \mathbf{x}^\top) + \sigma^2 I)^{-1} \mathbf{y} \quad (4)$$

$$\text{var}(y_*) = k(x_*, x_*) - K^\top(\mathbf{x}, x_*)(K(\mathbf{x}, \mathbf{x}^\top) + \sigma^2 I)^{-1} K(\mathbf{x}, x_*) \quad (5)$$

where \mathbf{x} is an input vector and \mathbf{y} is the observed value corresponding to input \mathbf{x} . Typically, GPs contain free parameters, called hyper-parameters, which can be optimized by minimizing the Negative Log Marginal Likelihood (NLML). The NLML is defined as follows:

$$\begin{aligned} NLML &= -\log p(\mathbf{y}|\mathbf{x}, \boldsymbol{\theta}) \\ &= \underbrace{\frac{1}{2} \mathbf{y}^\top (K + \sigma^2 I)^{-1} \mathbf{y}}_{\text{model fit}} + \underbrace{\frac{1}{2} \log |K + \sigma^2 I| + \frac{n}{2} \log(2\pi)}_{\text{complexity penalty}} \end{aligned} \quad (6)$$

where $K = K(\mathbf{x}, \mathbf{x}^\top)$, $\boldsymbol{\theta}$ are the hyper-parameters of the kernel function, and σ^2 is the noise level. The NLML above directly follows from the observation that $\mathbf{y} \sim N(0, K + \sigma^2 I)$.

In multi-output GPs (MOGPs), we have multiple sources of data which specify related outputs. The construction of the MOGP covariance function $k_{MOGP}(x^i, x^j)$ models covariances of each output and dependencies between pairs of different outputs [12].

2.2 Spectral mixture kernels

Usually, the smoothness and generalization properties of GPs depend on the kernel function and its hyper-parameters $\boldsymbol{\theta}$. Choosing an appropriate kernel function and its initial hyper-parameters based on prior knowledge from the data are the core steps of a GP. Various kernel functions have been proposed [2], such as Squared Exponential (SE), Periodic (PER), and general Matérn (MA). Recently new covariance kernels have been proposed in [9, 13], called Spectral Mixture (SM) kernels. An SM kernel, here denoted by k_{SM} , is derived through modeling a spectral density (Fourier transform of a kernel) with Gaussian mixtures. A desirable property of SM kernels is that they can be used to reconstruct other popular standard covariance kernels. According to Bochner's Theorem [14], the properties of a stationary kernel entirely depend on its spectral density. With enough components k_{SM} can approximate any stationary covariance kernel [13].

$$k_{SM}(\tau) = \sum_{q=1}^Q w_q \cos(2\pi \boldsymbol{\mu}_q \tau^\top) \prod_{p=1}^P \exp(-2\pi^2 \tau^2 \Sigma_q^{(p)}) \quad (7)$$

where Q is the number of components, P is the dimension of dataset, $w_q, \boldsymbol{\mu}_q = [\mu_q^{(1)}, \dots, \mu_q^{(P)}]$, and $\Sigma_q = \text{diag}([\sigma_q^{(1)2}, \dots, \sigma_q^{(P)2}])$ are weight, mean, and variance of the q th mixture component in frequency domain, respectively. The variance σ_q^2 can be thought of as an inverse length-scale, μ_q as a frequency, and w_q as a contribution.

Bochner's Theorem [14, 15] indicates a direction on how to construct a valid kernel from the frequency domain. This implies that these kind of kernels can also be transformed between time domain and frequency domain. Using the following definition, the spectral density of kernel function $k(\tau)$ can be given by its Fourier transform:

$$k^*(s) = \int_{-\infty}^{\infty} k(\tau) e^{-2\pi i \tau s} d\tau \quad (8)$$

Furthermore, the inverse Fourier transform of spectral density $k^*(s)$ is the original kernel function $k(\tau)$.

$$k(\tau) = \int_{-\infty}^{\infty} k^*(s) e^{2\pi i s \tau} ds \quad (9)$$

We will use a superscript asterisk $k^*(s)$ to denote the spectral density of a covariance function in the frequency domain. From Bochner's theorem [14, 15] $k(\tau)$ and $k^*(s)$ are Fourier duals of each other. For SM kernel [9], using Fourier transform of the spectral density $k^*(s) = [\phi(s) + \phi(-s)]/2$ where

$\phi(s) = \mathcal{N}(s; \boldsymbol{\mu}, \Sigma)$ is a symmetrized scale-location mixture of Gaussians in the frequency domain, we have

$$\begin{aligned} k_{SM}(\tau) &= \mathcal{F}_{s \rightarrow \tau}^{-1} \left[\sum_{q=1}^Q w_q k^*(s) \right] (\tau) \\ &= \sum_{q=1}^Q w_q \mathcal{F}_{s \rightarrow \tau}^{-1} [(\phi(s) + \phi(-s))/2] (\tau) \end{aligned} \quad (10)$$

3 Multi-output convolution spectral mixtures

We can now address the following questions. (1) How to construct cross spectral mixtures with time and phase delay through convolution? (2) How to extend the cross spectral mixtures to multi-output scenario? (3) What is the relationship between MOCSM and MOSM?

3.1 Time and phase dependent spectral mixture through convolution

Recently the GCSM [16] uses convolution to model spectral mixture level dependency. The cross covariance kernel function in GCSM between channels i and j is defined as follows:

$$\begin{aligned} k_{GCSM}^{i \times j}(\tau) &= \mathcal{F}_{s \rightarrow \tau}^{-1} [(g_{GCSM_i}^*(s) \cdot g_{GCSM_j}^*(s) + \overline{g_{GCSM_i}^*(s)} \cdot g_{GCSM_j}^*(-s))/2] (\tau) \\ &= \frac{(4\Sigma_i \Sigma_j)^{\frac{1}{4}}}{(\Sigma_i + \Sigma_j)^{\frac{1}{2}}} \exp \left(-\frac{(\boldsymbol{\mu}_i - \boldsymbol{\mu}_j)^2 + 4\pi^2 \Sigma_i \Sigma_j (2\tau - (\boldsymbol{\theta}_{tj} - \boldsymbol{\theta}_{ti}))^2}{4(\Sigma_i + \Sigma_j)} \right) \\ &\quad \times \cos \left(\pi \left(\frac{(\Sigma_i \mu_j + \Sigma_j \mu_i)(2\tau - (\boldsymbol{\theta}_{tj} - \boldsymbol{\theta}_{ti}))}{\Sigma_i + \Sigma_j} - (\theta_{pj} - \theta_{pi}) \right) \right) \end{aligned} \quad (11)$$

where

$$\begin{aligned} g_{GCSM_i}^*(s) &= \sqrt{\phi_{GCSM_i}(s)} \\ &= \left(\frac{1}{(2\pi)^P |\Sigma|} \right)^{\frac{1}{4}} \exp \left(-\frac{(s - \boldsymbol{\mu})^\top (s - \boldsymbol{\mu})}{4\Sigma} \right) \exp(-\pi \boldsymbol{\theta}_t s i - \pi \theta_p i) \end{aligned} \quad (12)$$

is a base spectral density of GCSM in the frequency domain and the overline denotes complex conjugate. When $P = 1$, $g_{GCSM_i}^*(s) = \left(\frac{1}{2\pi\sigma^2} \right)^{\frac{1}{4}} \exp(-\frac{(s-\mu)^2}{4\sigma^2}) \exp(-\pi\theta_t s i - \pi\theta_p i)$.

3.2 Multi-output convolution spectral mixture kernel

Motivated by the SM kernel and its spectral density formulation, if each channel has w_q weight in the original kernel spectral density, then the base spectral density of channel $g_{GCSM_i}^*(s) = \sqrt{w_i \phi_{GCSM_i}(s)}$, the cross spectral density between channels i and j is $g_{GCSM_i}^*(s) g_{GCSM_j}^*(s) = \sqrt{w_i w_j \phi_{GCSM_i}(s) \phi_{GCSM_j}(s)}$. In this case we have the cross convolution spectral kernel between channels i and j as follows:

$$\begin{aligned} k_{MOCSM}^{i \times j}(\tau) &= \sqrt{\frac{2w_i w_j \sigma_i \sigma_j}{\sigma_i^2 + \sigma_j^2}} \exp \left(-\frac{(\mu_i - \mu_j)^2 + 4\pi^2 \sigma_i^2 \sigma_j^2 (2\tau - (\theta_{tj} - \theta_{ti}))^2}{4(\sigma_i^2 + \sigma_j^2)} \right) \\ &\quad \times \cos \left(\pi \left(\frac{(\sigma_i^2 \mu_j + \sigma_j^2 \mu_i)(2\tau - (\theta_{tj} - \theta_{ti}))}{\sigma_i^2 + \sigma_j^2} - (\theta_{pj} - \theta_{pi}) \right) \right) \end{aligned} \quad (13)$$

where $\{i, j\} \in \{1, \dots, M\}$ are channel identifiers, θ_{ti} and θ_{pi} are time delay and phase delay of channel i , respectively. If there is no time and phase delay among channels, the cross convolution spectral kernel is only based on the convolution of ordinary base spectral mixtures and will be:

$$k_{MOCSM}^{i \times j}(\tau) = \sqrt{\frac{2w_i w_j \sigma_i \sigma_j}{\sigma_i^2 + \sigma_j^2}} \exp \left(-\frac{(\mu_i - \mu_j)^2 + 4\pi^2 \sigma_i^2 \sigma_j^2 \tau^2}{\sigma_i^2 + \sigma_j^2} \right) \cos \left(2\pi \tau \frac{\sigma_i^2 \mu_j + \sigma_j^2 \mu_i}{\sigma_i^2 + \sigma_j^2} \right) \quad (14)$$

Furthermore, when channel i is equivalent to channel j , we have

$$k_{MOCSM}^{i \times i}(\tau) = w_i \exp(-2\pi^2 \tau^2 \sigma_i^2) \cos(2\pi \tau \mu_i) \quad (15)$$

which shows that MOCSM is identical to the SM kernel with only one channel. However, up till now we only considered one component and one dimension. The MOCSM kernel with multiple components on multidimensional inputs is defined as

$$\begin{aligned} k_{MOCSM}^{i \times j}(\tau) &= \sum_{q=1}^Q \left(\Sigma_i^{(q)} \Sigma_j^{(q)} \right)^{\frac{1}{4}} \left(\frac{2w_i^{(q)} w_j^{(q)}}{\Sigma_i^{(q)} + \Sigma_j^{(q)}} \right)^{\frac{1}{2}} \\ &\times \exp \left(- \frac{(\boldsymbol{\mu}_i^{(q)} - \boldsymbol{\mu}_j^{(q)})^2 + 4\pi^2 \Sigma_i^{(q)} \Sigma_j^{(q)} (2\tau - (\boldsymbol{\theta}_{tj}^{(q)} - \boldsymbol{\theta}_{ti}^{(q)}))^2}{4(\Sigma_i^{(q)} + \Sigma_j^{(q)})} \right) \\ &\times \cos \left(\pi \left(\frac{(\Sigma_i^{(q)} \boldsymbol{\mu}_j^{(q)} + \Sigma_j^{(q)} \boldsymbol{\mu}_i^{(q)}) (2\tau - (\boldsymbol{\theta}_{tj}^{(q)} - \boldsymbol{\theta}_{ti}^{(q)}))}{\Sigma_i^{(q)} + \Sigma_j^{(q)}} - (\boldsymbol{\theta}_{pj}^{(q)} - \boldsymbol{\theta}_{pi}^{(q)}) \right) \right) \end{aligned} \quad (16)$$

In the MOCSM kernel, one can also employ angular frequencies instead of ordinary frequencies in the convolution and the inverse Fourier transform which results in

$$\begin{aligned} k_{MOCSM}^{i \times j}(\tau) &= \sum_{q=1}^Q \left(\Sigma_i^{(q)} \Sigma_j^{(q)} \right)^{\frac{1}{4}} \left(\frac{2w_i^{(q)} w_j^{(q)}}{\Sigma_i^{(q)} + \Sigma_j^{(q)}} \right)^{\frac{1}{2}} \\ &\times \exp \left(- \frac{(\boldsymbol{\mu}_i^{(q)} - \boldsymbol{\mu}_j^{(q)})^2 + 4\Sigma_i^{(q)} \Sigma_j^{(q)} (\tau - (\boldsymbol{\theta}_{tj}^{(q)} - \boldsymbol{\theta}_{ti}^{(q)}))^2}{4(\Sigma_i^{(q)} + \Sigma_j^{(q)})} \right) \\ &\times \cos \left(\frac{(\Sigma_i^{(q)} \boldsymbol{\mu}_j^{(q)} + \Sigma_j^{(q)} \boldsymbol{\mu}_i^{(q)}) (\tau - (\boldsymbol{\theta}_{tj}^{(q)} - \boldsymbol{\theta}_{ti}^{(q)}))}{\Sigma_i^{(q)} + \Sigma_j^{(q)}} - (\boldsymbol{\theta}_{pj}^{(q)} - \boldsymbol{\theta}_{pi}^{(q)}) \right) \end{aligned} \quad (17)$$

In above Equations (16) and (17), $\Sigma_i, \boldsymbol{\mu}_i, \boldsymbol{\theta}_{ti}, \boldsymbol{\theta}_{tj}$ have the same dimension P with Equation (7).

3.3 Comparison between MOCSM and MOSM

To simplify the comparison between MOCSM and MOSM and make the distinction more clear, we compare MOCSM and MOSM with only one component and one-dimensional input. In MOSM we have

$$\begin{aligned} k_{MOSM}^{i \times j}(\tau) &= 2w_i w_j \sqrt{\frac{\pi \sigma_i^2 \sigma_j^2}{\sigma_i^2 + \sigma_j^2}} \exp \left(- \frac{(\mu_i - \mu_j)^2 + 4\sigma_i^2 \sigma_j^2 (\tau + (\theta_{ti} - \theta_{tj}))^2}{4(\sigma_i^2 + \sigma_j^2)} \right) \\ &\times \cos \left(\frac{(\sigma_i^2 \mu_j + \sigma_j^2 \mu_i) (\tau + (\theta_{ti} - \theta_{tj}))}{\sigma_i^2 + \sigma_j^2} + (\theta_{pi} - \theta_{pj}) \right) \end{aligned} \quad (18)$$

Similarly, if there is no time and phase delay between channel i (output i) and channel j (output j), MOSM becomes

$$k_{MOSM}^{i \times j}(\tau) = 2w_i w_j \sqrt{\frac{\pi \sigma_i^2 \sigma_j^2}{\sigma_i^2 + \sigma_j^2}} \exp \left(- \frac{(\mu_i - \mu_j)^2 + 4\sigma_i^2 \sigma_j^2 \tau^2}{4(\sigma_i^2 + \sigma_j^2)} \right) \cos \left(\frac{\tau(\sigma_i^2 \mu_j + \sigma_j^2 \mu_i)}{\sigma_i^2 + \sigma_j^2} \right) \quad (19)$$

Furthermore, when channel i is equivalent to channel j we have

$$k_{MOSM}^{i \times i}(\tau) = w_i^2 \sqrt{2\pi \sigma_i^2} \exp \left(- \frac{1}{2} \sigma_i^2 \tau^2 \right) \cos(\mu_i \tau) \quad (20)$$

Here the spectral density of Equation (20) is not equal to the standard Gaussian distribution in the frequency domain. When we compare Equation (20) to the ordinary SM kernel, which, with angular frequencies, is defined as Equation (21) [3], it is clear that they are different.

$$k_{SM}^i(\tau) = w_i \exp \left(- \frac{1}{2} \sigma_i^2 \tau^2 \right) \cos(\mu_i \tau) \quad (21)$$

Table 1: Cross weight and its difference in MOSM and MOCSM.

Kernel	Single channel weight	Cross channel weight	Design method
SM	w_i	Not available	Bochner's Theorem
MOSM	$w_i^2 \sqrt{2\pi\sigma_i^2}$	$(4\pi w_i^2 w_j^2 \sigma_i^2 \sigma_j^2)^{\frac{1}{2}} (\sigma_i^2 + \sigma_j^2)^{-\frac{1}{2}}$	Matrices decomposition
MOCSM	w_i	$(2w_i w_j \sigma_i \sigma_j)^{\frac{1}{2}} (\sigma_i^2 + \sigma_j^2)^{-\frac{1}{2}}$	Spectral convolution

Particularly in Equation (20) the contribution (weight) term $w_i^2 \sqrt{2\pi\sigma_i^2}$ is mixed with w_i and σ_i , which produces inaccurate channel correlations. Comparing Equation (17) and Equation (18) we can observe that MOCSM and MOSM have the same *exp* terms and *cos* terms, but have different cross weight terms (see Table 1).

MOCSM and MOSM have the same parameter space, but the cross weights of MOCSM are more accurate. When weights (w_i, w_j) and variances (σ_i^2, σ_j^2) of channels are close to each other, in MOSM the cross weight term will amplify the cross correlation if $|w_i| > 1$, $|w_j| > 1$, $|\sigma_i| > 1$, and $|\sigma_j| > 1$, otherwise the cross weight term will shrink the cross correlation, since MOSM contains squared weights and variances (see Table 1).

In Figure 1 we illustrate this problematic behaviour of MOSM by setting the channel weights to $w = \{0.5, 0.6, 2.0, 2.1\}$ and channel variances to $\sigma^2 = \{0.4, 0.5, 2.0, 2.1\}$ corresponding to channel 1, channel 2, channel 3, and channel 4, respectively. The figure clearly shows that the cross weights in MOSM may be amplified or shrunk because of the square used in the cross channel weights. Therefore, in MOSM (second row), $\text{cov}(\text{channel}^{(1)}, \text{channel}^{(2)})$ (in red solid line) is smaller than MOCSM (in first row), $\text{cov}(\text{channel}^{(2)}, \text{channel}^{(3)})$ (in blue solid line) is larger than MOCSM, and particularly $\text{cov}(\text{channel}^{(3)}, \text{channel}^{(3)})$ (in green solid line) is much larger than MOCSM.

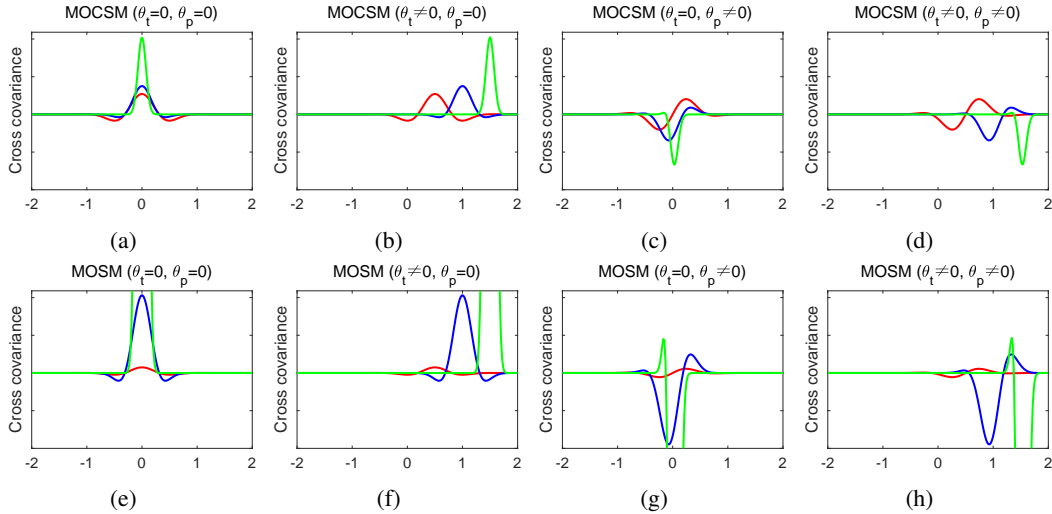


Figure 1: Cross covariances of K_{MOCSM} (first row) and K_{MOSM} (second row) with four channels. The columns show the channel dependencies with respect to zero time and phase delay, non-zero time delay and zero phase delay, zero time delay and non-zero phase delay, non-zero time and phase delay cross convolution. We only show three cross covariances: $\text{cov}(\text{channel}^{(1)}, \text{channel}^{(2)})$ with red solid line, $\text{cov}(\text{channel}^{(2)}, \text{channel}^{(3)})$ with blue solid line, $\text{cov}(\text{channel}^{(3)}, \text{channel}^{(4)})$ with green solid line.

4 Related work

There is an abundant literature on GPs related to MOGPs [3, 5, 7, 8, 10, 11, 17]. Here we mainly focus on MOGPs methods based on spectral mixture kernels, because of their expressiveness and recent

use in MOGPs. Since the introduction of SM kernels [9, 13], various MOGP methods have been introduced [9, 17, 18, 19, 20]. The first MOGPs based on the SM kernel is based on the framework of [10].

$$K_{SM-LMC} = \sum_{q=1}^Q B^q \otimes K_{SM}^q$$

The B^q in K_{SM-LMC} encodes cross weights to represent channel correlations and involves a linear combination of spectral mixtures. The CSM kernel [11] improved the expressivity of SM-LMC: it introduces a cross phase spectrum and is also defined within the LMC framework as

$$K_{CSM} = \sum_{q=1}^Q B^q K_{SG}(\tau; \theta^q)$$

where $B^q = \sum_{r=1}^{R_q} \beta_r^q (\beta_r^q)^\dagger$, $k_{SG}(\tau; \theta^q) = \exp(-\frac{1}{2}\nu^q \tau^2 + j\mu^q \tau)$, $\beta_r^{cq} = \sqrt{a_r^{cq}} \exp(-j\psi_r^{cq})$. However, the kernels K_{SG} used in the CSM are only phase dependent, but not time dependent. The more recent MOSM kernel [3] provided a principled framework to construct multivariate covariance functions with a better interpretation of cross correlations between channels. SM-LMC and CSM are instances of MOSM. However, MOSM cannot reduce to the SM kernel when using only one channel and in certain situations produces inaccurate channel correlations, for example, when patterns between channels are close to each other (see Table 1). More detailed comparisons between SM-LMC, CSM, MOSM, and MOCSM in terms of hyper-parameters and degrees of freedom are given in Table 2. In Table 2, all LMC use free form parameterization. For SM-LMC, CSM, MOSM and MOCSM, Q is the number of components, and M is the number of channels (outputs).

Table 2: Comparisons between MOCSM and other kernels [5].

Kernel	Parameters	Degrees of freedom
SE-LMC	$\{B, \theta_f, \theta_\ell\}$	$2 + (M^2 + M)/2$
Matérn-LMC	$\{B, \theta_f, \theta_\ell\}$	$2 + (M^2 + M)/2$
SM-LMC	$\{B_q, \mu_q, \sigma_q\}_{q=1}^Q$	$2Q + Q(M^2 + M)/2$
CSM	$\{\sigma_q, \mu_q, \{\mathbf{a}_q^r, \phi_q^r, \phi_{1q}^r \triangleq 0\}_{r=1}^M\}_{q=1}^Q$	$2Q + \sum_{q=1}^Q R_q(2Q - 1)$
MOSM	$\{\{w_m^q, \boldsymbol{\mu}_m^q, \Sigma_m^q, \boldsymbol{\theta}_{mt}^q, \theta_{mp}^q\}_{m=1}^M\}_{q=1}^Q$	$5MQ$
MOCSM	$\{\{w_m^q, \boldsymbol{\mu}_m^q, \Sigma_m^q, \boldsymbol{\theta}_{mt}^q, \theta_{mp}^q\}_{m=1}^M\}_{q=1}^Q$	$5MQ$

5 Experiments

We consider the empirical spectral density \mathbf{s} as derived from the data, and then applied a Bayesian Gaussian mixture model $p(\boldsymbol{\theta}|\mathbf{s}) = \sum_{i=1}^Q \tilde{w}_i \mathcal{N}(\tilde{\boldsymbol{\mu}}_i, \tilde{\Sigma}_i)$ in order to get the Q cluster centers of Gaussian spectral density. We use the Expectation Maximization algorithm [21] to estimate the parameters \tilde{w}_i , $\tilde{\boldsymbol{\mu}}_i$, and $\tilde{\Sigma}_i$. The results are used as initial values of w_i , $\boldsymbol{\mu}_i$, and Σ_i , respectively, for each channel in MOCSM.

We compare MOCSM with existing MOGP methods, namely SM-LMC, CSM, MOSM, on an artificial dataset and a real world dataset. First, we show the ability of MOCSM in modeling nonlinear correlated outputs simultaneously by considering a mixed signal sampled from a Gaussian distribution, its integral, and its derivative. Next, we use MOCSM for prediction tasks on a real world problem with three sensor array datasets related to climate change and air pollution monitoring: temperature evolution, sliding mean ozone concentration, and global radiation extrapolation. As performance metric we consider mean absolute error MAE = $\sum_{i=1}^n |y_i - \hat{y}_i|/n$. We implemented the model in Tensorflow [22] and GPflow [23] for its scalability and automatic differentiation routines.

5.1 Artificial data: learning nonlinear correlated mixed signals simultaneously

We designed an artificial experiment inspired by [3] but more complex, to model multiple non-linear correlated channels simultaneously. The three channels consist of a mixed signal, its integral, and

its derivative. Specifically, the signal of the first channel is sampled from $\mathcal{GP}(0, K_{SM})$ ($Q = 4$) with length 300 in the interval $[-10, 10]$, and then its first integral and derivative are numerically computed to be the signals of the second and third channel. This experiment is intended to validate the interpolation, extrapolation, and signal recovery ability of MOCSM as well as to compare its pattern recognition performance with that of other MOGP approaches. For the first channel, we randomly choose half of the data as training data, and the rest as test data. The integral signal in the interval $[-10, 0]$ is used for training (in gray), the rest of the signal is used for testing (in green). The derivative of the signal in the interval $[0, 10]$ is used for training and the rest of the signal is used for testing.

The performance of MOCSM (in dashed red line) on the first channel is shown in Figure 3 (a). Although MOCSM performed a bit better, the difference in performance among these methods is not so evident: all mentioned GP methods learned the covariance and interpolated the missing values well. Next, the extrapolation performance of MOCSM and other methods on the integral and the derivative of the signal are shown in Figure 3 (b) and Figure 3 (c), respectively. For instance, the integral of the signal contains more complex patterns, which is difficult to recognize and extrapolate. Here MOCSM performs better than other methods with lowest MAE (see Table 3) and smallest confidences interval.

Predictions obtained using SE-LMC and Matérn-LMC kernels are of low quality, especially for the extrapolation tasks (integral and derivative signals): it is very hard for them to find valid patterns in the data, like the evolution of trend over time. Overall, results on the artificial dataset indicate the capability of MOCSM to model integration and differentiation patterns of the generated signal simultaneously.

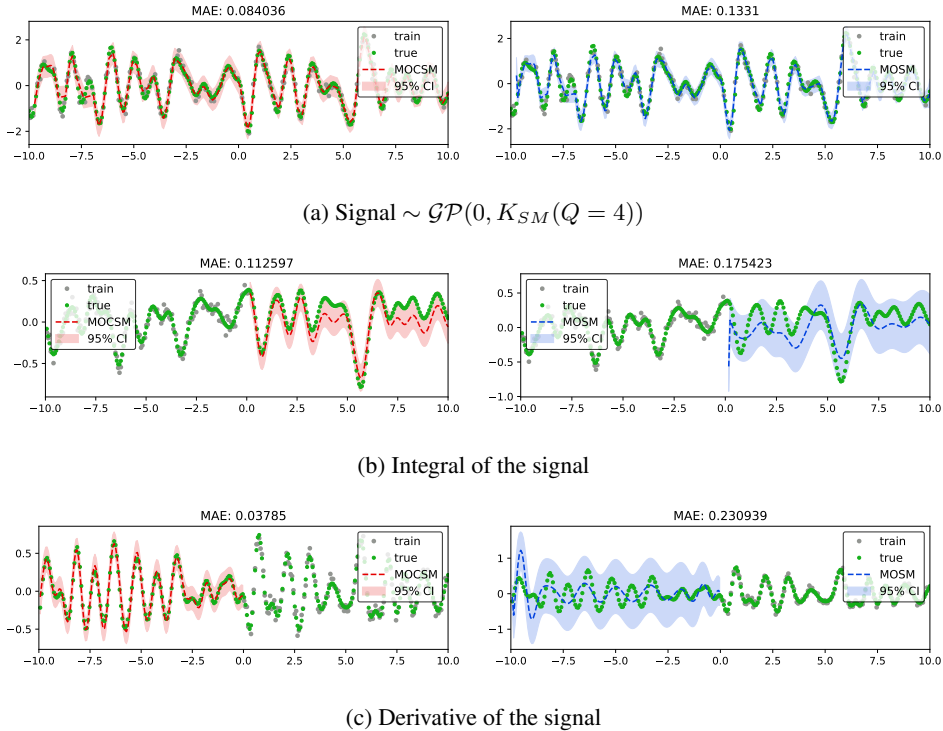


Figure 2: Performance of MOCSM (in red dashed line) and MOSM (in blue dashed line) on artificial dataset. (a) Signal sampled from $\mathcal{GP}(0, K_{SM})$ with $Q = 4$, training data are randomly chosen from the signal and the rest as test data. (b) Integral of the signal was numerically computed, the first half of data $x \in [-10, 0]$ was selected as a training and the remaining data as a test data. (c) Derivative of the signal was numerically computed, the last half of data $x \in [0, 10]$ was selected as a training and the rest as a test.

5.2 Temperature extrapolation

Sensor networks monitoring climate change and global warming in Stockholm¹ provide real time surveillance, historical analysis, and future forecasting of the regional environment. Particularly extrapolating future temperature values help to guide policy making and social development. We know that, as a result of global warming, the fluctuation of temperature becomes a sensitive topic with regard to balance of survival and development. On the other hand, temperature is one of main factors in affecting local air pollution levels because it determines chemical reaction and change of air pollutant. There are multiple global trends and local patterns which can shape temperature evolution. Global trends are natural evolution mechanisms within the global climate system itself. Local patterns are external forces caused by local surroundings and industry activities. Usually global trends affect long term evolution of temperature at a large scale. Local patterns always shape the short term and medium-term change of temperature at a small scale. Both global trends and local patterns are time and phase dependent and tightly coupled together. Here we use temperature recordings as a real world example to shows extrapolating ability of MOCSM in sensor networks. Based on the extrapolation results, suggestions may be given on measures to mitigate global warming.

The temperature monitoring recordings are recorded from a number of stations (Torkel Knutssongatan, Marsta, Norr Malma) in Stockholm and outside. For instance: Torkel Knutssongatan’s measurement at the urban background, Marsta’s measurement at a high-altitude tower, North Malma’s measurement at the regional background. We consider each station to be a channel: Torkel Knutssongatan as channel 1, Marsta as channel 2, and Norr Malma as channel 3. We observe from Figure 3 that the change of temperature has an apparent oscillatory behavior. In this case, we use temperature time series from 22 June 2017 to 12 July 2017, in 1 hour intervals. Here we just focus on the task in channel 2. Specifically, a randomly chosen half of the temperature data in Torkel Knutssongatan, the first half of the temperature data in Marsta, and the last half of the temperature data in Norr Malma are used for training. The last half of temperature data in Marsta is used for testing. The change of temperature in each channel is affected by their nonlinear interaction of time and phase related local patterns and global trends.

From Figure 3, as a result of time and phase dependent local patterns within channels (local patterns depend on surroundings) and time and phase dependent global trends between channels (global trends depend on seasonal or yearly factors), changes in temperature are fluctuating. MOCSM, however, consistently outperform others with lowest MAE and smallest predicted confidence interval (see Figure 3 and Table 3).

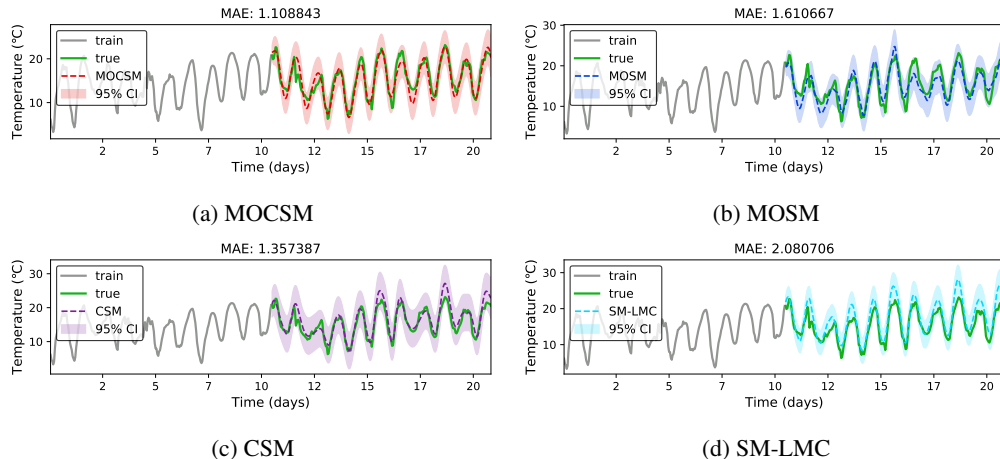


Figure 3: Temperature extrapolation. Performance comparison between MOCSM and recently proposed spectral mixture kernels: (a) MOCSM (in red dashed line), (b) MOSM (in blue dashed line), (c) CSM (in purple dashed line), (d) SM-LMC (in cyan dashed line).

¹<http://slb.nu/slbanalys/historiska-data-luft/>

5.3 Sliding mean Ozone concentration extrapolating

Secondly, we use an eight-hour average Ozone concentrations dataset. The Ozone dataset comes from an air pollution monitoring sensor network in Stockholm². The Ozone concentration is recorded from 5 April, 2017 to 25 April, 2017, in one-hour intervals at Torkel Knutssongatan, Norr Malma, and Hornsgatan stations. As a result of moving average, noise was smoothed and therefore the evolution of ozone concentration is more smooth and less fluctuant. In other words, patterns from the frequency domain should become more clear. However, Ozone concentration depends more on local environment and human activities. Thus its extrapolations is more difficult than temperature.

Although the Ozone concentration data was smoothed by a sliding window of 8-hour values, local patterns in each channel depending on surroundings and global trends related to large-scale climate change still exist. Both local patterns and global trends are time and phase dependent over the period of recording. Modeling from multiple channels can benefit the long range extrapolating rather than learning one channel alone, because the evolution of Ozone concentration in each station is a result of nonlinear interaction of these local patterns and global trends. Here randomly chosen half of data in Torkel Knutssongatan (channel 1), first half of data in Norr Malma (channel 2), and the last half of data in Hornsgatan (channel 3) are used for training and the remaining data in Norr Malma as a testing. In this case we still aim to extrapolate the long range trends of sliding mean Ozone concentration in Norr Malma. With the same setting in the first experiments, the performance of SM-LMC, CSM, MOSM, MOCSM are shown in Figure 4 and Table 3.

As seen in Figure 4, patterns in sliding mean Ozone concentration are more difficult and less clear to capture than temperature. It is even hard for human to find any quasi periodical or periodical trends. Although all MOGPs methods can extrapolate trends of sliding mean Ozone concentration, but MOCSM is the best, which be able to correctly predict the appearance of all low peaks and high peaks. No doubt MOCSM achieves better performance (see Figure 3 and Table 3) in terms of MAE and confidence interval. This experiment shows again that MOCSM has stronger pattern learning abilities.

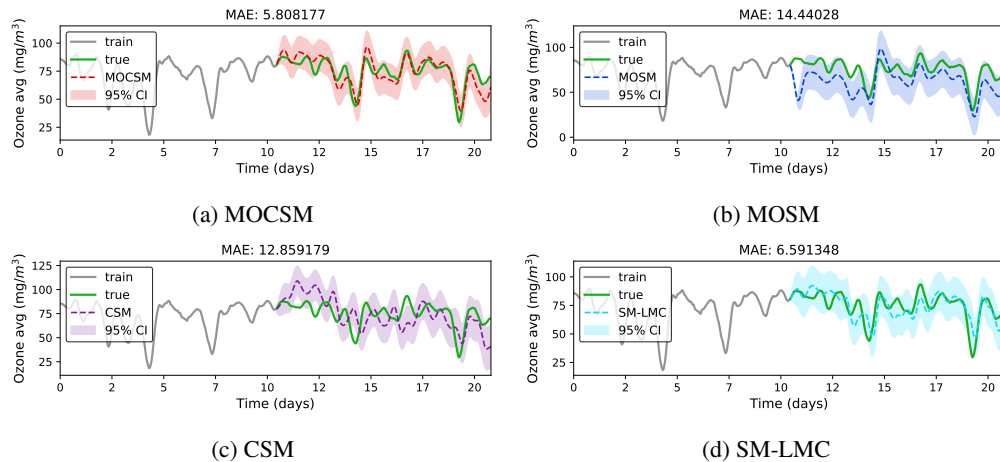


Figure 4: Sliding mean Ozone concentration extrapolation. Performance comparison between MOCSM and recently proposed spectral mixture kernels: (a) MOCSM (in red dashed line), (b) MOSM (in blue dashed line), (c) CSM (in purple dashed line), (d) SM-LMC (in cyan dashed line).

5.4 Global radiation backward extrapolation

After two extrapolating experiments, we conduct a backward extrapolation on global radiation recordings of the sensor networks in order to validate the long range back extrapolating capability and historical signal recovery ability of MOCSM and other methods. The global radiation is an important parameter reflecting global climate evolution and change of atmosphere. Global radiation is the total

²<http://slb.nu/slbanalys/historiska-data-luft/>

amount of direct, diffuse, and reflected solar energy received by the Earth’s surface, which is mainly affected by sun altitude and cloud cover.

The changes of sun altitude has a global influence on earth with a one-year period, while the cloud cover has a local influence with an a-periodic behavior. These global and local patterns show time and phase related variability over the period of recording. Usually for small scale variation (1 hour interval), the global radiation depends more on its surroundings and location because local weather condition determines the cloud cover. Empirical analysis shows various time and phase dependent characteristics of this global radiation: short term variations, medium term monthly patterns and non-strict periodic long term trends related to position of moon and sun, and some white noises. The time of appearance of high peak in global radiation is not periodical and its amplitude is always irregular.

The global radiation dataset is collected from three stations³ in Stockholm city: Torkel Knutssongatan’s measurement at urban background, Marsta’s measurement at a high-altitude tower, Norr Malma’s measurement at regional background. All recordings cover 24 hours at 1 hour intervals and missing values are filtered. In this case, we consider a global radiation recording from 5 December, 2017 to 26 December, 2017. Interestingly, the changing of global radiation over time looks like a non-continuous impulse signal because the sun radiation at night is almost equal to zero. From Figure 5 we can observe that the appearance of high peak in global radiation is irregular and its time of duration is short and fluctuant. Thus, complicated patterns contained in this non-continuous impulse signal is very difficult to detect. Ordinary kernels cannot find any valid patterns in this dataset. In a multi-output scenario, the changing of global radiation in each channel is caused by their nonlinear interaction of time and phase related local and global patterns.

In our experiment, we randomly choose half of global radiation data in Torkel Knutssongatan, the first half of global radiation data in Marsta, and the last half of global radiation data in Norr Malma as training data in channel 1, channel 2, and channel 3, respectively. Different from the first and second real world experiment, the rest of the Norr Malma time series is used for testing. In this setting, MOCSM consistently outperforms the other baselines with a lower MAE (see Figure 5 and Table 3). Results indicate that all methods have difficulty to capture the trends of high peak appearance, and only MOCSM can forecast it without over estimation.

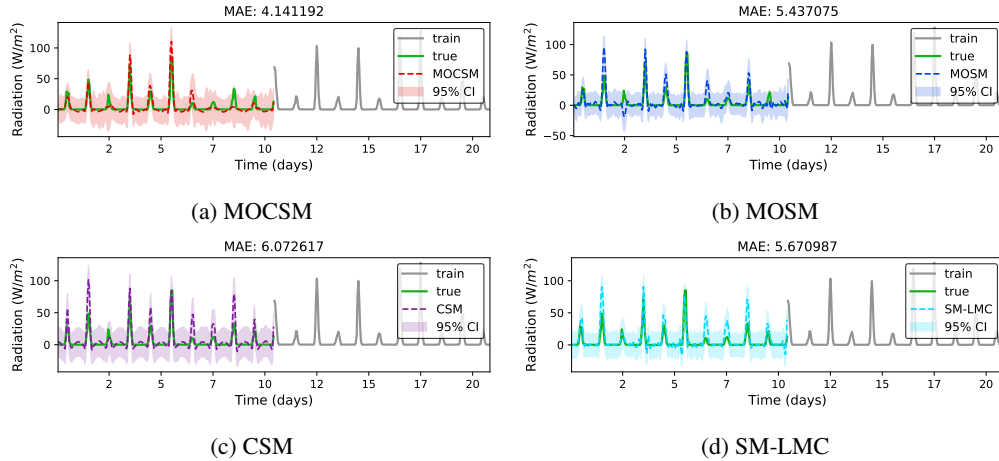


Figure 5: Global radiation back extrapolation. Performance comparison between MOCSM and recently proposed spectral mixture kernels: (a) MOCSM (in red dashed line), (b) MOSM (in blue dashed line), (c) CSM (in purple dashed line), (d) SM-LMC (in cyan dashed line).

Table 3 summarizes the performance of the considered kernel methods. The MOCSM kernel consistently achieves the lowest MAE on the artificial and the real world datasets. Predictions obtained using the SE-LMC and Matérn-LMC kernels are very bad especially for extrapolation (Integral, Derivative signals, Temperature, and Sliding mean Ozone concentration) even if the methods achieve a good MAE. With these kernels it is very hard to find any valid pattern in the data.

³<http://slb.nu/slbanalys/historiska-data-luft/>

Table 3: Performance of MOCSM and other kernels on artificial and real world datasets.

Kernel	$\mathcal{GP}(0, K_{SM})$	Integral	Derivative	Temperature	Ozone	Radiation
SE-LMC	0.156	0.225	0.212	13.677	62.154	5.499
Matérn-LMC	0.126	0.219	0.221	14.737	70.867	5.230
SM-LMC	0.124	0.195	0.195	2.081	6.591	5.671
CSM	0.128	0.200	0.210	1.357	12.859	6.072
MOSM	0.133	0.175	0.231	1.611	14.440	5.437
MOCSM	0.084	0.113	0.038	1.109	5.808	4.141

We use the temperature in Marsta, the sliding mean Ozone concentration in Norr Malma, and the radiation in Norr Malma as tasks to perform long range extrapolation.

6 Conclusion

We proposed the generalized multi-output convolution spectral mixture (MOCSM) kernel with expressive closed form to describe cross covariance between multi-outputs in a principled way. In our method we incorporated time and phase delay in spectral density, then transform convolution into product through Fourier transform.

MOCSM shows stronger abilities in modeling complicated nonlinear correlation across multi-outputs than the considered baselines. Experiments on artificial datasets and real world datasets have shown that by using cross convolution of spectral mixtures within MOGPs, more irregular trends in the data can be recognized and learnt and long-term trends forecasting and long range back extrapolation can be performed in a more accurate way.

For example, they can be applied to fill in the gaps that cross correlations are not so precise in MOSM, and extend the extrapolating ability of MOSM without increasing complexity in training and inference steps. In this work we did not address efficient inference of the MOCSM. At present, efficient inference approximation methods like FITC and PITC [8, 24, 25, 26, 27, 28, 29], are not very effective for MOGPs. Interesting future research involves the development of sparse and efficient inference methods for MTGPs [30, 31, 32].

Global optimizing and initialization strategy of hyper-paramters are also very important for the MOGP performance. Here we considered the empirical spectral density as derived from the data, and then applied a Bayesian Gaussian mixture model. More advanced initialization strategies, like [20, 33, 34, 35] need to be investigated in future work.

Acknowledgement

This work was partly supported by China Scholarship Council (CSC).

References

- [1] C. E. Rasmussen and H. Nickisch, “Gaussian processes for machine learning (gpml) toolbox,” *Journal of Machine Learning Research*, vol. 11, no. Nov, pp. 3011–3015, 2010.
- [2] C. E. Rasmussen, *Gaussian processes for machine learning*, ser. Adaptive computation and machine learning, C. K. I. Williams, Ed. Cambridge, Massachusetts: The MIT Press, 2006, hier auch später erschienene, unveränderte Nachdrucke.
- [3] G. Parra and F. Tobar, “Spectral mixture kernels for multi-output Gaussian processes,” in *Advances in Neural Information Processing Systems*, 2017, pp. 6684–6693.
- [4] P. Goovaerts, “Geostatistics for natural resources evaluation. oxford univ. press, new york.” *Geostatistics for natural resources evaluation. Oxford Univ. Press, New York.*, 1997.
- [5] E. V. Bonilla, K. M. Chai, and C. Williams, “Multi-task Gaussian process prediction,” in *Advances in neural information processing systems*, 2008, pp. 153–160.
- [6] R. Dürichen, M. A. Pimentel, L. Clifton, A. Schweikard, and D. A. Clifton, “Multitask Gaussian processes for multivariate physiological time-series analysis,” *IEEE Transactions on Biomedical Engineering*, vol. 62, no. 1, pp. 314–322, 2015.
- [7] A. Melkumyan and F. Ramos, “Multi-kernel Gaussian processes,” in *IJCAI Proceedings-International Joint Conference on Artificial Intelligence*, vol. 22, no. 1, 2011, p. 1408.
- [8] M. Alvarez and N. D. Lawrence, “Sparse convolved Gaussian processes for multi-output regression,” in *Advances in neural information processing systems*, 2009, pp. 57–64.
- [9] A. G. Wilson, “Covariance kernels for fast automatic pattern discovery and extrapolation with Gaussian processes,” *University of Cambridge*, 2014.
- [10] A. G. Wilson, D. A. Knowles, and Z. Ghahramani, “Gaussian process regression networks,” *arXiv preprint arXiv:1110.4411*, 2011.
- [11] K. R. Ulrich, D. E. Carlson, K. Dzirasa, and L. Carin, “GP kernels for cross-spectrum analysis,” in *Advances in neural information processing systems*, 2015, pp. 1999–2007.
- [12] M. G. Genton and W. Kleiber, “Cross-covariance functions for multivariate geostatistics,” vol. 30, pp. 147–163, 2015.
- [13] A. Wilson and R. Adams, “Gaussian process kernels for pattern discovery and extrapolation,” in *Proceedings of the 30th International Conference on Machine Learning (ICML-13)*, 2013, pp. 1067–1075.
- [14] S. Bochner, *Lectures on Fourier Integrals.(AM-42)*. Princeton University Press, 2016, vol. 42.
- [15] M. Stein, “Interpolation of spatial data: some theory for kriging. 1999.”
- [16] K. Chen, P. Groot, J. Chen, and E. Marchiori, “Spectral Mixture Kernels with Time and Phase Delay Dependencies,” *ArXiv e-prints*, Aug. 2018.
- [17] D. Duvenaud, J. R. Lloyd, R. Grosse, J. B. Tenenbaum, and Z. Ghahramani, “Structure discovery in nonparametric regression through compositional kernel search,” *arXiv preprint arXiv:1302.4922*, 2013.
- [18] S. Flaxman, A. Wilson, D. Neill, H. Nickisch, and A. Smola, “Fast kronecker inference in Gaussian processes with non-Gaussian likelihoods,” in *International Conference on Machine Learning*, 2015, pp. 607–616.
- [19] J. B. Oliva, A. Dubey, A. G. Wilson, B. Póczos, J. Schneider, and E. P. Xing, “Bayesian nonparametric kernel-learning,” in *Artificial Intelligence and Statistics*, 2016, pp. 1078–1086.
- [20] P. A. Jang, A. Loeb, M. Davidow, and A. G. Wilson, “Scalable Levy process priors for spectral kernel learning,” in *Advances in Neural Information Processing Systems*, 2017, pp. 3943–3952.
- [21] T. K. Moon, “The expectation-maximization algorithm,” *IEEE Signal Processing Magazine*, vol. 13, no. 6, pp. 47–60, 1997.
- [22] M. Abadi, P. Barham, J. Chen, Z. Chen, A. Davis, J. Dean, M. Devin, S. Ghemawat, G. Irving, M. Isard *et al.*, “Tensorflow: A system for large-scale machine learning. arxiv preprint,” *arXiv preprint arXiv:1605.08695*, 2016.

- [23] A. G. d. G. Matthews, M. van der Wilk, T. Nickson, K. Fujii, A. Boukouvalas, P. León-Villagrà, Z. Ghahramani, and J. Hensman, “GPflow: A Gaussian process library using tensorflow,” *Journal of Machine Learning Research*, vol. 18, no. 40, pp. 1–6, 2017.
- [24] M. Álvarez, D. Luengo, M. Titsias, and N. Lawrence, “Efficient multioutput Gaussian processes through variational inducing kernels,” in *Proceedings of the Thirteenth International Conference on Artificial Intelligence and Statistics*, 2010, pp. 25–32.
- [25] M. A. Álvarez and N. D. Lawrence, “Computationally efficient convolved multiple output Gaussian processes,” *Journal of Machine Learning Research*, vol. 12, no. May, pp. 1459–1500, 2011.
- [26] C. K. Williams and M. Seeger, “Using the nystrom method to speed up kernel machines,” in *Advances in neural information processing systems*, 2001, pp. 682–688.
- [27] J. Quiñonero-Candela and C. E. Rasmussen, “A unifying view of sparse approximate Gaussian process regression,” *Journal of Machine Learning Research*, vol. 6, no. Dec, pp. 1939–1959, 2005.
- [28] E. Snelson and Z. Ghahramani, “Sparse Gaussian processes using pseudo-inputs,” in *Advances in neural information processing systems*, 2006, pp. 1257–1264.
- [29] K. Chalupka, C. K. Williams, and I. Murray, “A framework for evaluating approximation methods for Gaussian process regression,” *Journal of Machine Learning Research*, vol. 14, no. Feb, pp. 333–350, 2013.
- [30] B. Rakitsch, C. Lippert, K. Borgwardt, and O. Stegle, “It is all in the noise: Efficient multi-task Gaussian process inference with structured residuals,” in *Advances in neural information processing systems*, 2013, pp. 1466–1474.
- [31] C. Guarnizo and M. A. Álvarez, “Fast kernel approximations for latent force models and convolved multiple-output Gaussian processes,” *arXiv preprint arXiv:1805.07460*, 2018.
- [32] H. Liu, Y.-S. Ong, X. Shen, and J. Cai, “When Gaussian process meets big data: A review of scalable GPs,” *arXiv preprint arXiv:1807.01065*, 2018.
- [33] K. Swersky, J. Snoek, and R. P. Adams, “Multi-task Bayesian optimization,” in *Advances in neural information processing systems*, 2013, pp. 2004–2012.
- [34] R. Martinez-Cantin, “Bayesopt: A Bayesian optimization library for nonlinear optimization, experimental design and bandits,” *The Journal of Machine Learning Research*, vol. 15, no. 1, pp. 3735–3739, 2014.
- [35] N. Knudde, J. van der Herten, T. Dhaene, and I. Couckuyt, “GPflowopt: A Bayesian optimization library using tensorflow,” *arXiv preprint arXiv:1711.03845*, 2017.